Flow, Turbulence and Combustion 2005 **74:** 67–84

Efficient Generation of Initial- and Inflow-Conditions for Transient Turbulent Flows in Arbitrary Geometries

ANDREAS KEMPF, MARKUS KLEIN and JOHANNES JANICKA
Institute for Energy and Powerplant Technology, Department of Mechanical Engineering, Darmstadt Technical University, Peterstenstrasse 30, 64287 Darmstadt, Germany; E-mail: kleinm@ekt.tu-darmstadt.de

Received 3 November 2003; accepted in revised form 11 July 2004

Abstract. A method is presented to artificially generate initial conditions and transient inflow-conditions for DNS and LES. It creates velocity fields that satisfy a given Reynolds-stress-tensor and length-scale. Compared to existing approaches, the new method features greater flexibility, efficiency and applicability. It is well suited for the complex geometries and for the arbitrary grids that occur in technical applications. This is demonstrated in connection with the generation of initial data for an internal combustion engine. To assess the accuracy and efficiency of the new approach, it is applied to the test-case of a non-premixed jet-flame, which is known to be sensitive to transient inflow-data.

Key words: inflow conditions, initial conditions, LES, DNS, inflow-generation.

1. Introduction

The fluid flow in a domain strongly depends on the location and the type of the boundaries. On these boundaries, adequate conditions must be set for all transported scalars and velocity components. Hence, the turbulence properties must be prescribed. With the classical Reynolds Averaged Navier-Stokes (RANS)-approach, this requires to set the proper mean velocities and the transported turbulence quantities such as turbulent kinetic energy k or the components of the Reynolds-stress-tensor $\langle u_i u_j \rangle$ and its rate of dissipation ϵ. These quantities can be determined with moderate experimental effort or may be estimated.

With the powerful approaches of Direct Numerical Simulation (DNS) or Large Eddy Simulation (LES), the turbulent fluctuation is no longer described by simple, steady, transported quantities. Instead, the turbulent fluctuations are resolved, which leads to transient, fluctuating velocity fields. On the inflow, these fluctuations must be prescribed to perform a comprehensive DNS/LES. This leads to a vicious circle, since the transient flow-field on the inflow must be known *prior* to the simulation. To solve this problem, much work was spent by many groups. For recent work, see [2, 24]. Klein et al. [12] provides an overview of these methods that is resumed here.

Bonnet et al. [4] use experimentally determined time-series and correlation functions to obtain the inflow-conditions. The approach is very expensive and cannot provide any predictive ability. The actual system must be built before the flow can be "post-predicted".

In many cases, the computational domain can be extended upstream of the area of interest. This only works if the relevant turbulent structures are produced inside the additional domain. This approach requires much additional computer power – eventually even more than is required for the area of interest.

The best way to break the above-mentioned vicious circle is to eliminate the inflow-boundaries by applying periodic boundary conditions. The approach is limited to simple geometries but may be extended to spatially developing flows by coordinate transformations as suggested by [25]. However, periodic boundary conditions disturb the large-scale structures by enforcing spatial periodicity, as discussed by [15].

In many configurations, a long pipe delivers the fluid to the nozzle. The computational domain can then be chosen such that the inflow-boundary is on the nozzle-exit plane. In this case, periodic boundary conditions can be applied to simulate the fully developed turbulent flow established upstream of the inflow-plane. This precursor simulation yields a flow-field of which slices are stored and used as inflow-data.

In general, inflow-conditions from auxiliary simulations are too expensive if not impossible. Then, turbulent inflow-data can be generated by superimposing fluctuations to the mean velocities. In the most simple case, these fluctuations consist of random noise which is scaled to satisfy the trace elements of the Reynolds-stress-tensor $\langle u_i u_j \rangle$. Unfortunately, noise introduces too much energy in the high wave number range, so that the prescribed pseudo-turbulence is damped immediately. This leads to similar results as obtained with steady inflow-conditions. However, a proposal by [14] improves on this significantly.

Klein et al. [12] suggested an effective method to generate turbulent inflow-velocities that satisfy a given Reynolds-stress-tensor and a given length-scale. With this procedure, specifying the inflow-turbulence for LES/DNS becomes as simple as with for Reynolds-stress models. However, the approach is only efficient with simple grids. The extension to complex geometries is too complicated to retain the full advantages of this simple, efficient procedure.

In the present paper, a methodology is presented that seizes on the mentioned approach. The new method is easy to apply for arbitrary geometries and unstructured grids. It even allows the effortless extension of an existing CFD-code to create its own turbulent initial conditions.

Before presenting the new approach for creating inflow-data, some LES-theory and numerics are repeated. Then, some established methods for generating turbulent inflow-conditions are explained, before the new approach is shown. Its abilities are assessed for the test-case of a turbulent non-premixed flame, its simplicity is shown for an internal combustion engine. To improve the readability of the paper,

mathematical derivations were neglected in the main paper. They are discussed in Appendix instead.

2. Governing Equations and Modeling

This paper presents a method that generates artificial inflow-boundary conditions for LES/DNS. This section resumes the underlying theory for LES and DNS. Since the new methodology will be assessed for turbulent non-premixed flames, the very basics of combustion modeling must be presented here as well.

2.1. FILTERING (LES)

The accurate transport equation for a given quantity Φ comprises the full spectrum of length-scales, which is considered by a DNS. In contrast, LES describes the large-scale features only, which are extracted by spatial low-pass filtering of the Φ field. Transport equations for the filtered $\overline{\Phi(x_j,t)}$ field are obtained by filtering the accurate transport equations. The difference between the filtered field $\overline{\Phi(x_j,t)}$ and the original field $\Phi(x_j,t)$ is the unresolved "fine-structure" $\Phi'(x_j,t)$. This work applies a top-hat filter that is based on the computational cell. With the finite volume approach, this "Schumann-filter" [22] simplifies the numerical procedure. Schumann-filtering happens implicitly when the values at the center of a cell as well as the face averages are approximated by the mean value for the whole cell.

The filtering of the governing equations yields unknown correlations $\overline{\varrho\Phi}$ with the density ϱ. For Favre-filtered quantities $\tilde{\Phi} = \overline{\varrho\Phi}/\bar{\varrho}$, these correlations are already known: $\overline{\varrho\Phi} = \tilde{\Phi}\bar{\varrho}$

When the filter-width Δ is reduced to zero, the filtered fields converge into the accurate fields. Hence, the filtered (LES) equations feature the accurate (DNS) equations when the filterwidth is zero. Then, the model-contributions τ_{kk} and ν_t vanish and the equations are accurate again.

2.2. TRANSPORT EQUATIONS

To compute the transient development of turbulent reactive flows, we solve the transport Equations (1, 2, 3) for the (Favre) filtered density $\bar{\rho}$, velocity $\tilde{u}_i$ and mixture-fraction $\tilde{f}$.

$$\frac{\partial\bar{\varrho}}{\partial t} + \frac{\partial}{\partial x_j}(\bar{\varrho}\widetilde{u_j}) = 0 \tag{1}$$

$$\frac{\partial}{\partial t}(\bar{\varrho}\tilde{u}_i) + \frac{\partial}{\partial x_j}(\bar{\varrho}\tilde{u}_i\widetilde{u_j}) = \frac{\partial}{\partial x_j}\left[\bar{\varrho}(\nu_t+\nu)\left(\frac{\partial\widetilde{u_j}}{\partial x_i} + \frac{\partial\tilde{u}_i}{\partial x_j}\right) - \frac{2}{3}\bar{\varrho}(\nu_t+\nu)\frac{\partial\widetilde{u_k}}{\partial x_k}\delta_{ij}\right] - \frac{1}{3}\frac{\partial}{\partial x_i}\bar{\varrho}\tau_{kk}^{\mathrm{sgs}} + \frac{\partial\bar{p}}{\partial x_i} + \bar{\varrho}g_i \tag{2}$$

$$\frac{\partial}{\partial t}(\bar{\varrho}\tilde{f}) + \frac{\partial}{\partial x_j}(\bar{\varrho}\tilde{f}\tilde{u}_j) = \frac{\partial}{\partial x_j}\left(\bar{\varrho}\left(\frac{\nu_t}{\sigma_t} + \frac{\tilde{\nu}}{\sigma}\right)\frac{\partial \tilde{f}}{\partial x_j}\right) \tag{3}$$

The continuity Equation (1) is identical to the unfiltered equation but is only solved in terms of filtered quantities. The modeled transport Equation (2) for momentum (Navier-Stokes equation) features the filtered pressure $\bar{p}$ and the negative buoyancy $\bar{\rho} g_i$. The sub-grid-contribution to the momentum flux is modeled by the eddy viscosity ν_t and the trace of the sub-grid-stress tensor τ_{kk}^{sgs}. In Equation (3) for the filtered mixture fraction $\tilde{f}$, the sub-grid-contribution to the fluxes is modeled with the eddy-diffusivity (ν_t/σ_t), which is computed from the turbulent Schmidt number ($\sigma_t = 0.45$, following [20]). The turbulent viscosity ν_t in Equations (2) and (3) is modeled following Smagorinsky's suggestion (4) [23]. The parameter C_s is taken from the dynamic Germano procedure [4] and the filter-width is denoted by Δ.

$$\nu_t = (C_s \Delta)^2 \left| \frac{1}{2}\left(\frac{\partial \widetilde{u_j}}{\partial x_i} + \frac{\partial \tilde{u}_i}{\partial x_j}\right)\right| \tag{4}$$

The trace of the sub-grid-stress tensor τ_{kk}^{sgs} can be discarded in Equation (2) by introducing the pressure parameter $\bar{P} = \bar{p} - 1/3\bar{\varrho}\tau_{kk}^{\text{sgs}}$. This pressure parameter $\bar{P}$ is determined from the pressure correction scheme.

2.3. Modeling of combustion

This work determines the chemical state from the mixture-fraction. It is defined as the local ratio of mass from the fuel-stream to the overall mass and varies from zero (air) to one (fuel). In this work, Bilger's definition [3] for the reaction of hydrocarbons and oxygen is applied.

From mixture-fraction f, the species mass-fractions x_α are computed with the steady flamelet Equation (5). In this equation, S_{x_α} denotes the chemical source-terms provided by the reaction mechanism. The scalar rate of dissipation χ depends on the coefficient of diffusion (ν/σ) and the mixture-fraction field f.

$$-\varrho\frac{\chi}{2}\frac{\partial^2 x_\alpha}{\partial f^2} = S_{x_\alpha} \quad \text{with} \quad \chi = 2\frac{\nu}{\sigma}\left(\frac{\partial f}{\partial x_j}\frac{\partial f}{\partial x_j}\right) \tag{5}$$

Solving Equation (5), the species concentrations x_α, the temperature, the density and the viscosity are functions of the mixture-fraction f and the scalar rate of dissipation χ only.

In LES, just the filtered mixture fraction $\tilde{f}$ and scalar rate of dissipation $\tilde{\chi}$ are known. However, the dependent quantities Φ (e.g. x_α, ϱ) are nonlinear functions of f and χ. Hence, the sub-grid-distribution of f and χ must be considered since $\tilde{\Phi}(f, \chi) \neq \Phi(\tilde{f}, \tilde{\chi})$. The sub-grid-distribution of the mixture fraction is described by a presumed β-PDF, which is a function of the sub-grid-variance $\widetilde{f''^2}$ and $\tilde{f}$. The sub-grid-distribution of the scalar rate of dissipation, which is generally thought to

obey a log-normal law, is described by a simple Dirac function δ here. Then, all dependent scalars can be computed by $\tilde{\Phi}(f, \chi) = \Phi(\tilde{f}, \tilde{\chi}, \widetilde{f''^2})$. This function is pre-integrated and tabulated, so $\tilde{\Phi}$ is simply determined by interpolation from the table.

The sub-grid-variance in the mixture-fraction $\widetilde{f''^2}$ is modeled as the resolved variance $\widehat{(\tilde{f})''^2}$ in a test-filter cell $\hat{\mathrm{C}}$ of twice the volume of cell C. This model was suggested and applied by Forkel and shows very good numerical properties. This model is described in much greater detail in [7]. The filtered scalar rate of dissipation $\tilde{\chi}$ is determined according to the model by [6], relying on an eddy-viscosity approach.

2.4. Numerical procedure

Following Forkel et al. [8], the conservation equations for mass $\bar{\varrho}$ (1), momentum $\overline{\varrho u_i}$ (2) and mixture $\overline{\varrho f}$ (3) were transformed to cylindrical coordinates (x, r, ϕ) and discretized in space by finite volumes.

Time-integration by an explicit three-step low-storage Runge-Kutta scheme [27] advances the solution from time-step n to $n+1$. For the scalars, each Runge-Kutta sub-step m features a prediction- and a correction-step to deal with the nonlinear dependency $\bar{\varrho}^{m+1} = \bar{\varrho}(\tilde{f}^{m+1}, \tilde{\chi}^{m+1}, \widetilde{f''^2}^{m+1})$. In the predictor-step, $\bar{\varrho}^m$ and $\overline{\varrho f}^m$ are transported to yield $\tilde{f}^{m+1} = \overline{\varrho f}^{m+1}/\bar{\varrho}^{m+1^*}$. For this mixture-fraction field $\tilde{f}^{m+1}$, the chemistry-table yields the correct new density $\bar{\varrho}_c^{m+1}$. The difference between the densities $\bar{\varrho}^{m+1^*}$ and $\bar{\varrho}_c^{m+1}$ must be eliminated by the pressure correction scheme. This adapts the velocities in such a way that transport of $\bar{\varrho}^m$ would yield $\bar{\varrho}^{m+1} = \bar{\varrho}_c^{m+1}$ instead of $\bar{\varrho}^{m+1^*}$. In the correction step, $\bar{\varrho}^m$ and $\overline{\varrho f}^m$ are actually transported with the corrected velocities, resulting in the new solutions $\bar{\varrho}^{m+1}$ and $\overline{\varrho f}^{m+1}$. Since this scheme only transports conserved scalars $\bar{\varrho}$ and $\overline{\varrho f}$, it could be implemented in a fully conservative way. Hence, this scheme was named "Echt Konservativer Transport" (EKT, fully conservative transport).

Diffusive fluxes of scalars and momentum were discretized by second-order central schemes. For convection, second-order central schemes were only applied to momentum to minimize numerical dissipation. The fluxes of $\bar{\varrho}$ and $\overline{\varrho f}$ were discretized by a TVD scheme, which inhibits numerical oscillations without introducing strong numerical diffusion.

3. Generation of Inflow Conditions

The common approach to generate pseudo-turbulent velocity fields in 3D superimposes a field of random fluctuation $u_i'(x_j, t)$ to the mean velocity field $\langle u_i \rangle(x_j)$. The generation of the fluctuation field u_i' consists of (1) generating fluctuating signals $\mathcal{U}_i$ (see Sections 3.1–3.4) and (2) transforming them to u_i' in a way to satisfy the Reynolds-stress-tensor (see Section 3.5). The resulting 3D velocity field is then used to extract the inflow-data.

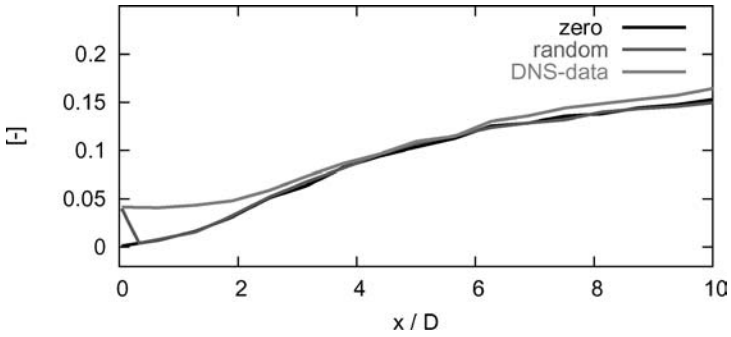

Figure 1. Normalized fluctuation of the axial velocity $\sqrt{\overline{u'u'}}/\overline{U_{\mathrm{cl}}}$ plot along the centerline. There is no difference between results for inflow data with zero fluctuation and with random noise. The inflow-turbulence extracted from DNS-data is maintained.

3.1. GENERATING FLUCTUATIONS BY RANDOM NOISE

The most simple way of generating fluctuating signal fields $\mathcal{U}_i$ is to apply random noise. This means that the signal on each node is just determined as a random number. Investigations by [12, 17] revealed that this method generates turbulence that is immediately dampened to zero right after the inflow-plane. This is explained by the relative lack of energy in the low-wave number range since random noise possesses an energy spectrum of the form $E(k) = \text{const}$.

This effect was shown for the DNS of a plane turbulent jet [12]. Figure 1 gives the velocity fluctuation along the centerline of the jet. Results obtained for the noise inflow-condition are compared to data for a laminar (steady) inflow and for precomputed turbulence. The noise-condition yields a proper fluctuation-level on the inflow, but is then dissipated immediately.

3.2. GENERATING FLUCTUATIONS BY FOURIER TRANSFORM

To overcome the problem of too much energy on high-wave numbers, Lee et al. [14] suggested to apply an inverse Fourier transformation using an energy-spectrum of real turbulence.

For illustration we focus on a 1D example. The Fourier transformation of a signal u_k in physical space to a signal U_n in wave number space reads:

$$u_k = \frac{1}{N} \sum_{n=0}^{N-1} U_n e^{\frac{2\pi i k n}{N}} \tag{6}$$

Here, U_n ($n \in \{0, \ldots, N-1\}$) are complex numbers $U_n = |U_n| * e^{i\Phi_n}$ having a phase angle of Φ_n. The energy of this signal U_n is given by:

$$\sum_{n=0}^{N-1} E(n) := \frac{1}{N} \sum_{n=0}^{N-1} |U_n|^2 = \sum_{i=0}^{N-1} |u_i|^2 \tag{7}$$

This yields a connection between the absolute value of U_n and the energy spectrum $E(n)^{1/2} \sim |U_n|$. With a random phase angle Φ_n, the inverse Fourier Transform yields finally a signal field which features the prescribed spectrum $E(n)$.

This method was tested in simulations by [13, 12, 21] and others. However, the method is complicated and hard to implement. Furthermore, it requires equidistant, Cartesian grids. Finally, the method is based on three-dimensional energy spectra which are on the one hand hard to determine experimentally and must on the other hand be prescribed globally.

3.3. Generating fluctuations by digital filters

To overcome some of these difficulties, Klein et al. [12] applied digital filters to generate the signal fields $\mathcal{U}_i$, based on suggestions from [18]. The method was developed having applicability and simplicity in mind. It is able to generate pseudo-turbulent velocity data with a prescribed Reynolds-stress-tensor and a locally defined autocorrelation function.

In 1D, a series r_m of random data with $\overline{r_m} = 0, \overline{r_m r_m} = 1$ is created first. The signal r_m is convoluted with a digital, linear, non-recursive filter according to Equation (8). In this equation, b_n denotes the filter-coefficients and $2N + 1$ gives the width of the filter-kernel.

$$u_m = \sum_{n=-N}^{N} b_n r_{m+n} \tag{8}$$

The definition is extended to 3D by the convolution of three one-dimensional filters, which yields the three-dimensional filter: $b_{ijk} = b_i \cdot b_j \cdot b_k$.

For random data we have $\overline{r_m r_n} = 0$ for $m \neq n$. Based on this observation and on formula (8) [12] gives a nonlinear implicit relation for the filter coefficients' dependency on the desired autocorrelation function R_{uu} of u_m. This equation can for example be solved by a Newton method or by a further simplification proposed in Reference [12].

3.4. New approach: Generating fluctuations by diffusion

The development of the established approaches (from random noise to Fourier transform to digital filters) shows a significant improvement in terms of accuracy and applicability. However, even the filtering technique requires equidistant grid spacing.

A new approach has been developed to generate inflow-conditions, which is based on physical space and easy to apply and implement with any CFD code. It relies on a diffusion process that converts white noise into a signal that features the required length-scale.

In a first step, again, three fields of random noise $\mathcal{U}_i$ are generated. These are normalized to fulfill $\bar{\mathcal{U}}_i = 0$ and $\overline{\mathcal{U}_i \mathcal{U}_i} = 1$. To compensate for the effect of cell-size, these fields are scaled by the inverse square-root of the volume $V_{\mathbf{i}}$ of cell $\mathbf{i} = (i_x, i_y, i_z)$. This heuristic scaling is motivated (for 1D) in the corollary of Appendix.

$$\mathcal{U}_{i,\mathbf{i}} := \frac{1}{\sqrt{V_{\mathbf{i}}}} \mathcal{U}_{i,\mathbf{i}} \tag{9}$$

The signal-fields do not feature reasonable autocorrelations yet. The typical length-scale is approximately half the extent of a cell. In the subsequent step, the small structures in the fields $\mathcal{U}_i$ are removed by applying diffusion, so that the large-scale structures become dominant.

$$\frac{\partial \mathcal{U}_i}{\partial t} = D \frac{\partial^2 U_i}{\partial x_j^2} \tag{10}$$

For a given coefficient of diffusion D, the length-scale increases with the time for which diffusion is applied. The length-scale L develops according to the following equation:

$$L \approx \sqrt{2\pi c n}\, \Delta x \quad \text{with} \quad c = D \frac{\Delta t}{\Delta x^2} \tag{11}$$

This is shown with the corollary in Appendix. In this Equation (11), Δt denotes to the width of a time-step, Δx to the width of a cell and n to the number of time-steps.

Theorem 2 of Appendix shows that diffusion is equivalent to the convolution of the original signal with a Gauss-Filter. This process yields an autocorrelation function of Gaussian shape (see Theorem 1 in Appendix). For the case of homogeneous turbulence in a late stage, it can be shown [5] that the autocorrelation function takes for a fixed time the form

$$R_{uu}(r, 0, 0) = \exp\left(-\frac{\pi}{4} \frac{r^2}{L^2}\right) \qquad (\text{with } L = L(t) = \sqrt{2\pi \nu (t - t_0)}), \tag{12}$$

which demonstrates a posteriori that the spectral content of the generated velocity data is reasonable.

Finally, the signal fields $\mathcal{U}_i$ must be normalized again to reestablish the properties $\bar{\mathcal{U}}_i = 0$ and $\overline{\mathcal{U}_i \mathcal{U}_i} = 1$.

Since diffusion occurs in physical space, it can be applied to arbitrary grids. The implementation of this process in a CFD code is straight-forward since CFD codes feature diffusive transport anyway.

Figure 2 (left) shows a slice of a typical signal-field in 3D. It was created on a cylindrical mesh with 80 nodes in radial and 128 nodes in circumferential direction. The radius of the domain was 0.1, the length-scale 0.0075. In the center of the domain, where the grid-cells are small, the structures are well resolved. Away

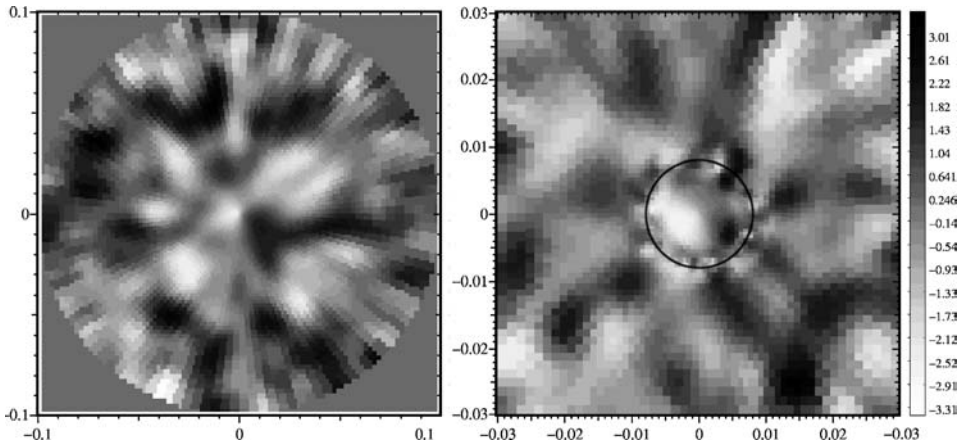

Figure 2. Signal-fields created on a cylindrical mesh (80 nodes radial, 128 nodes circumferential). Left: A constant length-scale of 0.0075 was applied to the whole domain. On cylindrical grids, resolution degrades with radius. A zero-gradient condition was applied to the annular surface. Right: Inhomogeneous length-scale-field on a cylindrical grid. A pipe is located in coaxial coflow. Inside the pipe, the length-scales are proportional to the distance from the wall. Outside, the length-scales were limited to 0.004.

from the axis, the grid-resolution is coarser. Yet, the approach yields reasonable data even for this region. At the annular surface, a zero-gradient condition was applied.

Certainly, the new approach is not restricted to constant length-scales. Inhomogeneous length-scale fields can be obtained by just applying an inhomogeneous diffusion coefficient field. As well, the diffusion process may be stopped locally as soon as the required length-scale is obtained, whereas in other regions, diffusion is continued. This ability to vary the length-scale is of particular importance close to walls, where the length-scale is proportional to the distance from the wall (mixing-length assumption). Such a signal-field is shown in Figure 2 (right). It shows a signal field created for a pipe in coaxial flow. The length-scale equals the distance from the wall (black) of a pipe, but was limited to the radius (0.004) of the pipe.

3.5. SATISFYING THE REYNOLDS-STRESS-TENSOR

All the three velocity fluctuation fields u_i' are based on the signal fields $\mathcal{U}_i$. These fields are normalized to a mean value of $\bar{\mathcal{U}}_i = 0$ and to correlations $\overline{\mathcal{U}_i \mathcal{U}_j} = \delta_{ij}$.

The velocity fluctuation fields u_i' are then constructed from the given Reynolds-stress-tensor R_{ij}. To only satisfy the trace elements, it is sufficient to determine the fluctuations as $u_\alpha' = {R_{\alpha\alpha}}^{1/2} \mathcal{U}_\alpha$. However, the cross-correlations can easily be set as well following a procedure by Lund et al. [16]. With the tensor a_{ij} (Equation (13),

u_i' can be determined as $u_i' = a_{ij}\,\mathcal{U}_j$.

$$a_{ij} = \begin{bmatrix} R_{11}^{0.5} & 0 & 0 \\ R_{21}/a_{11} & \left(R_{22} - a_{21}^2\right)^{0.5} & 0 \\ R_{31}/a_{11} & \left(R_{32} - a_{21}a_{31}\right)/a_{22} & \left(R_{33} - a_{31}^2 - a_{32}^2\right)^{0.5} \end{bmatrix} \tag{13}$$

Following this procedure, a pseudo-turbulent velocity field u_i is created. Slices of this can be extracted and applied as inflow-data to the LES, by using Taylor's hypothesis.

Sofar, the pseudo-turbulent velocity field u_i is not divergence free. However, in the case of inflow data, one cannot speak of divergence because the derivative in axial direction is not defined. Therefore by default our velocity field is not divergence free. But like in [14], it would be easily possible to generate a three-dimensional field and then to perform a projection. The authors did not find significant disadvantages when neglecting the divergence condition (in the sense of Taylor's hypothesis). However, the situation might be different for compressible codes. For iterative solvers, it is advised to apply a correction to the mass flow at the inlet, which is very easy to achieve. According to our experience, the correction amount to no more than 1% of the stream wise velocity.

3.6. Flow chart for proposed algorithm

An algorithm for generating inflow data with the proposed method may look like this:

(a) Choose a diffusion coefficient D, an appropriate time-step Δt, and the number of iterations to achieve the desired length-scale (see Equation (11) and Appendix corollary)
(b) Initialize and store three random fields $\mathcal{R}_\alpha$, $\alpha = x, y, z$ with the dimensions of the computational grid in the inflow plane. In the third direction the number of grid points should be large enough to avoid the introduction of low frequencies by going periodically through the domain.
(c) Multiply the random fields $\mathcal{R}_\alpha$, $\alpha = x, y, z$ at each node $\mathbf{i}$ with $\sqrt{V_\mathbf{i}}$.
(d) Apply the diffusion for the number of time-steps determined in (a).
(e) Normalize $\mathcal{R}_\alpha$ to a mean value of $\bar{\mathcal{U}}_i = 0$ and to correlations $\overline{\mathcal{U}_i\mathcal{U}_j} = \delta_{ij}$. The result yields the three-dimensional arrays of spatially correlated data $\mathcal{U}_\alpha$, $\alpha = x, y, z$
(f) Perform Lund's coordinate transformation (Equation (13)). Then, $u_\alpha(i, j, k)$ has the desired Reynolds-stresses.
(g) Slices of this can be extracted and applied as inflow-data to the LES/DNS, by going periodically through the domain using Taylors hypothesis.

3.7. Generating initial conditions at 'no effort'

Although the new approach to generate boundary conditions can be easily implemented into any CFD-code, it can yield turbulent initial conditions for an even smaller effort. For example, it allows to generate "homogeneous turbulence in a box" at almost no cost at all – with any CFD-code.

At first, the velocity fields u_i are initialized with the mean velocities and some superimposed noise of a predetermined level (see Appendix). Then, time-integration is performed, yet without pressure correction. Turning off the pressure correction is important since pressure correction tends to "destroy" most of the noise applied.

Time integration diffuses the noise since convection (without any mean velocity imposed) will hardly contribute to the transport. After some time-steps, the velocity fields will feature the appropriate length-scale. Finally, the desired mean velocities are superimposed onto the velocity fluctuations and the normal time-integration (including pressure correction) is started up. Depending on the code, an additional projection step may be required before the simulation is started up.

Obviously, this simplified method leads so far to uncorrelated velocity fields ($R_{ij} = 0$ for $i \neq j$). Of course, Lunds procedure [16] could be applied, but in many cases, this will not be necessary. In particular, since the new method only requires to (1) initialize the velocity with arbitrary values and to (2) turn of the pressure correction. These "abilities" should exist in any code!

3.8. Validation of the new approach

The new approach must be validated for a set of meaningful test-cases. Complex configurations are presented in Section 4, which considers an axis-symmetric turbulent reactive jet and an internal combustion engine.

For a more basic examination, the results obtained by [12] can be transfused. Their work considers artificially generated initial and boundary conditions for a plane channel flow, for a plane jet, and for the two-dimensional breakup of a liquid jet. As shown in the appendix, the diffusion approach yields a gaussian shape of the autocorrelation function. Therefore, in the case of Cartesian grids, the results from the diffusion approach contain identically the same spectral information as the digital filter approach (with the special choice of filter coefficients proposed in [12]). Therefore, it is not necessary to repeat the validation for simple geometries.

Figure 3 shows one-dimensional field of random numbers that has been diffused and filtered, respectively. The results can hardly be distinguished, confirming that the diffusion method works as well as the filtering technique.

4. Application of the New Approach

In this section, the new method is applied to two test-cases. First, artificial velocity data in a pipe is created to be used as inlet data for a non-premixed jet-flame. The

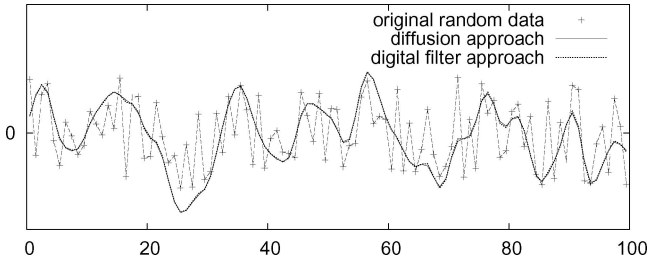

Figure 3. A random noise signal of 99 samples. The lines show the fields resulting from diffusion and from filtering. The difference is negligible.

sensitivity of the flow to the boundary condition is pointed out. A second test-case demonstrates the generality of the method by creating initial data for an internal combustion engine.

4.1. GENERATION OF INLET DATA FOR A NON-PREMIXED JET-FLAME

The new approach can improve the prediction of technical flows significantly. A non-premixed jet-flame is investigated to show the importance of accurate inflow-data and to examine the effects of varying inflow length-scales.

The test-flame (Tacke HD) was already investigated by [26] and [11]. The burner (EKT Standardbrenner [19]) consists of a pipe that ejects the nitrogen (77% vol.) diluted hydrogen (23% vol.) fuel at 36.3 m/s. The pipe is 8 mm in diameter D and long enough to ensure fully developed turbulence at a Reynolds number of $Re = 16{,}000$. A wind-tunnel generates a coaxial laminar co-flow of air at 0.2 m/s.

The computational domain of 15 D in radial and 16.7 D in axial direction is resolved by $190 \times 45 \times 32$ nodes (ax., rad., circ.). Transient inflow-profiles determined by the inflow-data generator were forced on the inflow-plane. The mixture-fraction was set to 1 within the nozzle-radius and 0 outside. To reduce numerical oscillation and to improve accuracy, the mixture-fraction profile was smeared over one cell. On the outflow-plane, von Neumann conditions were applied to all quantities. On the annular surface, pressure and mixture fraction were set 0, whereas for momentum, a simplified equation is solved to allow for entrainment.

Simulations were performed for six different length-scale profiles. In each case, the integral length-scale L was set to

$$L = c\,\Delta y, \tag{14}$$

where Δy is the distance from the wall. The parameter was set $c \in \{\, 0.0, 0.2, 0.4, 0.6, 0.8, 1.0\}$.

Instantaneous snapshots of the density-fields for different length-scales are shown in Figure 4. Comparison reveals how strongly the larger scales destabilize the jet and contribute to break-up.

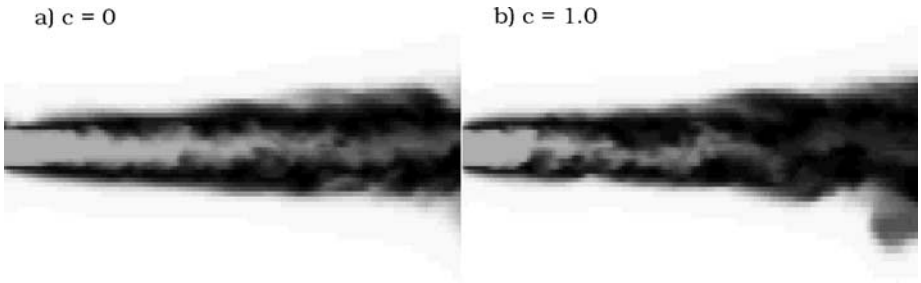

Figure 4. Instantaneous snapshots of the density-fields resulting from a small length-scale (a) and a large length-scale (b). Note that large length-scales make the jet break-up closer to the nozzle (left edge of each picture). White color represents air, black color burned gasses. No interpolation was applied in post-processing, the picture shows the actual mesh.

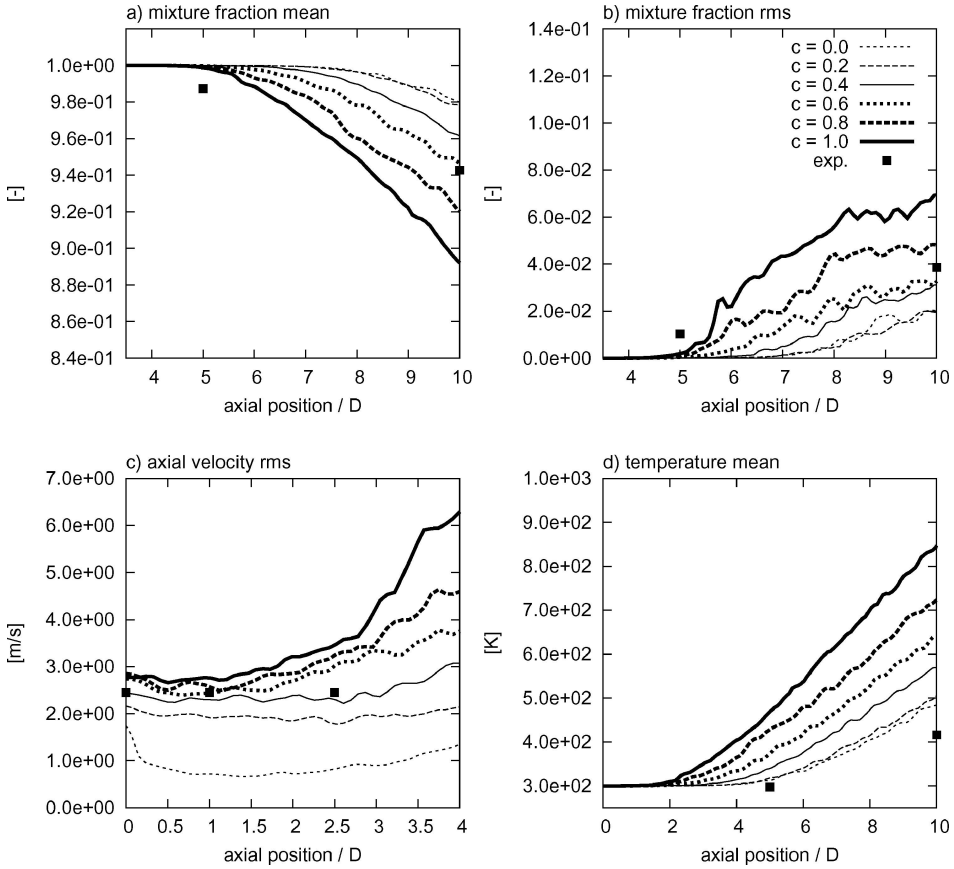

Figure 5. Various quantities along the centerline for smallest ($c = 0$) to largest ($c = 1$) length-scale (see formula (14)). Mixture-fraction mean (a), mixture-fraction fluctuation (b), axial velocity rms (c) and temperature mean (d).

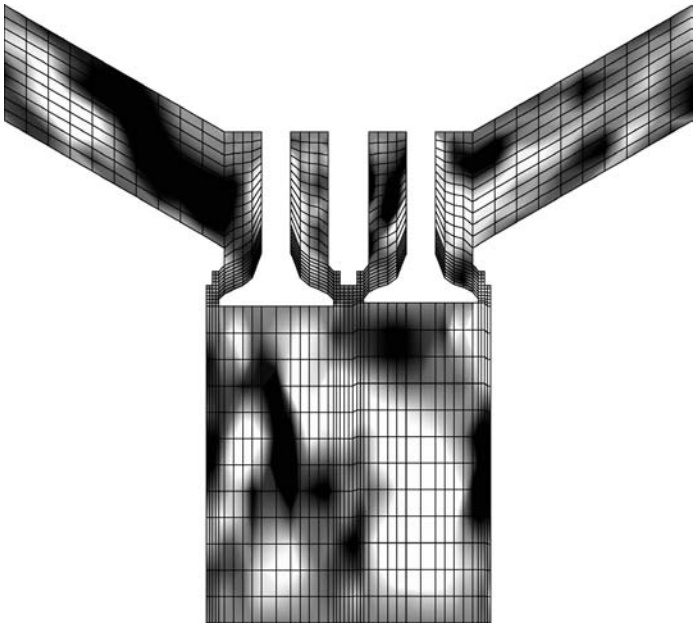

Figure 6. Initial conditions generated on the complex mesh of an internal combustion engine. The gray-level gives the fluctuation superimposed to one velocity component.

Figure 5 presents the development of the main quantities along the centerline. The lines show the simulations performed for varying length-scales, the points give the experimental data. Figure 5a shows that the decay of the mixture-fraction mean increases with length-scale. This represents stronger spreading of the jet. As well, growing length-scales shift the point of jet-break-up towards the nozzle. The same trends are observed in the mixture-fraction fluctuation (Figure 5b). Figure 5c shows how dissipation at the inflow is affected by the length-scale: large-scale structures vanish less rapidly than small-scale structures. For random-noise ($c = 0$), most of the energy vanishes within the first cells. Hence, large structures can destabilize the flow much more efficiently. Finally, Figure 5d shows how the temperature mean is affected by the inflow-data. In this region, the simulation over-predicts the experimental data. This was expected since the steady-flamelet chemistry-model neglects kinetic effects, which are important in the nozzle-region.

To conclude, the test-flame was found to be very sensitive on the length-scale of the inflow-data. A reasonable prediction is only possible if proper inflow-data is prescribed.

4.2. Generation of initial data for an internal combustion engine

So far the inflow generator has been used for a cylindrical grid, which poses much more problems than a Cartesian equidistant mesh. However, it is not arbitrary as

stated in the title of the paper. To show that the proposed method works with arbitrary meshes as well, it has been implemented into the KIVA code [1] to generate initial data for an internal combustion engine. Since this test only serves for illustration, a coarse grid was chosen and the length-scales were set to be large. Figure 6 shows the applicability of this approach. It should be stressed that the implementation of this approach into the KIVA code just required one day of work.

5. Conclusions

A method was presented to artificially generate initial conditions and transient inflow-conditions for DNS and LES. This method yields fluctuating velocity fields that both satisfy prescribed integral length-scales and Reynolds-stress-sensors. The new method features great flexibility, efficiency and applicability. Its effects on a flow-simulation were shown for the example of a turbulent reactive jet. This confirms that for many relevant simulations, proper length-scales must be prescribed. Although this may be complicated with classical methods, it can easily be achieved with the approach presented in this paper. In a second test-case we generated initial data for an internal combustion engine. The implementation of the method into the KIVA code [1] took only one day. This demonstrates the simplicity of the proposed method and its applicability to arbitrary geometries.

Acknowledgements

The authors gratefully acknowledge the financial support by the DFG (German Research Council) Sonderforschungsbereich 568 "Flow and Combustion in Future Gas Turbine Combustion Chambers". Furthermore, the authors want to thank Dmitry Goryntsev for generating initial data in an internal combustion engine.

Appendix: Mathematical Considerations

THEOREM 1. *The convolution of a white noise signal u with zero mean and unit variance with a gauss filter of the form*

$$g(x) = \frac{1}{\sqrt{4\pi Dt}} \exp\left(- \frac{x^2}{4Dt} \right) \tag{15}$$

yields a normalized autocorrelation function which has the following shape

$$R_{u*g,u*g}(r, t) = \exp\left(- \frac{r^2}{8Dt} \right). \tag{16}$$

Proof. Let u be a random signal, so that the (not normalized) autocorrelation

$$\int_{-\infty}^{\infty} u(x)\, u(x+r)\, \mathrm{d}x = C\delta(r) \tag{17}$$

is a Dirac function, where the parameter C is obviously connected to the variance of the signal. Furthermore the Fourier transform is denoted by

$$\mathcal{FT}(f)(k) = \int_{-\infty}^{\infty} f(x) \exp(-2\pi i k x)\, \mathrm{d}x \tag{18}$$

Using the following transform pairs [10]

$$\delta(x),\ \exp(-x^2/a^2) \Leftrightarrow \text{const.},\ \sqrt{\pi}a \exp(-\pi^2 k^2 a^2) \tag{19}$$

$$af + bh \Leftrightarrow a\mathcal{FT}(f) + b\mathcal{FT}(h) \tag{20}$$

$$(f * h) \Leftrightarrow \mathcal{FT}(f) \cdot \mathcal{FT}(h) \tag{21}$$

$$\mathrm{corr}(f, h) \Leftrightarrow \mathcal{FT}(f) \cdot \overline{\mathcal{FT}(h)} \tag{22}$$

where

$$(f * h)(x) := \int_{-\infty}^{\infty} f(x - x')h(x')\, \mathrm{d}x' \tag{23}$$

$$\mathrm{corr}(f, h)(x) := \int_{-\infty}^{\infty} f(x' + x)h(x')\, \mathrm{d}x' \tag{24}$$

it can be seen:

$$\begin{aligned}
&\int_{-\infty}^{\infty} (u * g)(x)\, (u * g)(x + r)\, \mathrm{d}x \\
&\overset{(22)}{=} \mathcal{FT}^{-1}\{\mathcal{FT}(u * g)\, \overline{\mathcal{FT}(u * g)}\} \overset{(21)}{=} \mathcal{FT}^{-1}\{\mathcal{FT}(u)\overline{\mathcal{FT}(u)}\, \mathcal{FT}(g)\overline{\mathcal{FT}(g)}\} \\
&\overset{(22)}{=} \mathcal{FT}^{-1}\{\mathcal{FT}(\mathrm{corr}(u, u))\, |\mathcal{FT}(g)|^2\} \overset{(17,19,20)}{=} C \cdot \mathcal{FT}^{-1}\{\mathcal{FT}(g)^2\} \\
&\overset{(15,19,20)}{=} C \cdot \mathcal{FT}^{-1}\{\exp(-\pi^2 k^2 8Dt)\} \overset{(19)}{=} C \cdot \frac{1}{\sqrt{8\pi Dt}} \cdot \exp\left(-\frac{r^2}{8Dt}\right)
\end{aligned}$$

□

THEOREM 2. *The solution to the following equation*

$$\frac{\partial u}{\partial t} = D\Delta u, \quad u(x, 0) = u_0(x), \quad x \in \mathbb{R} \tag{25}$$

which describes a homogeneous diffusion process, is equivalent to a convolution of $u_0(x)$ with a Gaussian smoothing filter and

$$u(x, t) = \frac{1}{\sqrt{4\pi Dt}} \exp\left(-\frac{x^2}{4Dt}\right) * u_0(x) \tag{26}$$

Proof. Fourier transforming Equation (25) yields a linear first-order differential equation which can easily be solved and back transformed [10]. □

COROLLARY. *Let u_i^0 be a discrete random signal with zero mean and unit variance and u_i^n the discrete solution of Equation* (25). *Furthermore let $\Delta x_i = \text{const.}$ and $\Delta t_n = \text{const.}$. Then the discrete correlation $\overline{u_i^n u_{i+k}^n}/\overline{u_i^n u_i^n}$ can be approximated by*

$$\frac{\overline{u_i^n u_{i+k}^n}}{\overline{u_i^n u_i^n}} \approx \exp\left(-\frac{k^2}{8cn}\right) \text{ with } c := \frac{D\Delta t}{\Delta x^2} \tag{27}$$

It follows for the length-scale $L \approx \sqrt{2\pi cn}\,\Delta x$.

If Equation (25) *is discretized, e.g. in time with an explicit Euler scheme and in space with central differences, it can be shown that the fluctuation level develops proportional to $\sqrt{\Delta x}$.*

Proof. The first part of the corollary follows immediately from Theorems 1 and 2. For the second part we obtain obviously the following iteration scheme

$$u_i^{n+1} := (1 - 2 * c)u_i^n + c\left(u_{i-1}^n + u_{i+1}^n\right) \tag{28}$$

which is described by the single parameter c. Inspecting again the proof of Theorem 1 and setting $k = 0$ we obtain

$$\left(\overline{u_i^n u_i^n}\right)^{1/2} \sim \left(\frac{1}{\sqrt{8\pi D\Delta t\, n}}\right)^{1/2}. \tag{29}$$

Changing D in Equation (28), is equivalent to changing $1/\Delta x^2$, because of the definition of c. Therefore Equation (29) shows that the numerically obtained value of $(\overline{u_i^n u_i^n})^{1/2}$ scales as $\sqrt{\Delta x}$. □

References

1. Amsden, A., O'Rourke, P. and Butler, T., *KIVA-II: A Computer Program for Chemically Reactive Flows with Sprays*. Los Alamos National Laboratory (1989).
2. Batten, P., Goldberg, G. and Chakravarthy, S., *Using Synthetic Turbulence to Interface RANS and LES*. 41st Aerospace Sciences Meeting and Exhibit, Reno, US (2003), AIAA 2003-81.
3. Bilger, R., Starner, S. and Kee, R., On reduced mechanisms for methane–air combustion in nonpremixed flames. *Combust. Flame* **80** (1990) 135–149.
4. Bonnet, J., Moser, R. and Rodi, W., AGARD Advisory Report 345, *A Selection of Test Cases for the Validation of Large Eddy Simulations of Turbulent Flows*. AGARD 1998, 7 Rue Ancelle, 99200 Neuilly-sur-Seine, France (1998), Ch. 6.3 Jets, p. 35.
5. Batchelor, G.K., *The Theory of Homogeneous Turbulence*. Cambridge University Press (1953).
6. Cook, A. and Riley, J., A subgrid model for equilibrium chemistry in turbulent flows. *Phys. Fluids* **6**(8) (1994) 2868–2870.

7. Forkel, H., Über die Grobstruktursimulation turbulenter Wasserstoff-Diffusionsflammen. Doctoral Thesis, TU-Darmstadt, VDI-Verlag, Fortschritt-Berichte, Reihe 6, Nr. 428, Düsseldorf, Germany (1999).
8. Forkel, H. and Janicka, J., Large eddy simulation of a turbulent hydrogen diffusion flame. *Flow, Turbulence Combust.* **65** (2000) 163–175.
9. Germano, M., Piomelli, U., Moin, P. and Cabot, W., A dynamic subgrid-scale eddy viscosity model. *Phys. Fluids A* **3** (1991) 1760–1765.
10. Jähne, B., *Digital Image Processing*. Springer (2002).
11. Kempf, A., Sadiki, A. and Janicka, J., Prediction of finite chemistry effects using large eddy simulation. *Proc. Combust. Inst.* **29** (2002) 1979–1985.
12. Klein, M., Sadiki, A. and Janicka J., A digital filter based generation of inflow data for spatially developing direct numerical or large eddy simulations. *J. Comp. Phys.* **186** (2002) 652–665.
13. Le, H. and Moin, P., Direct numerical simulation of turbulent flow over a backward-facing step. Technical Report TF-58, Stanford University (1994).
14. Lee, S., Lele, S. and Moin, P., Simulation of spatially evolving compressible turbulence and application of Taylors hypothesis. *Phys. Fluids* **A4** (1992) 1521–1530.
15. Lygren, M. and Anderson, H., Influence of boundary conditions on the large scale structures in turbulent plane couette flow. In: Banerjee, S. and Eaton, J. (eds.), *Turbulence and Shear Flow 1*. Begell House (1999) 15–20.
16. Lund, T., Wu, X. and Squires, D., Generation of turbulent inflow data for spatially-developing boundary layer simulations. *J. Comp. Phys.* **140** (1998) 233–258.
17. Mengler, C., Heinrich, C., Sadiki, A. and Janicka, J., Numerical prediction of momentum and scalar fields in a jet in cross flow: Comparison of LES and second order turbulence closure calculations. In: TSFP-2, Vol. II. Stockholm (2001) pp. 425–430.
18. Nobach, H., Verarbeitung stochastisch abgetasteter Signale. Ph.D. Thesis, University of Rostock, Germany (1997).
19. Pfuderer, D., Neubert, A., Früchtel, G., Hassel, E. and Janicka, J., Turbulence modulation in jet diffusion flame: Modeling and experiments. *Combust. Flame* **106**(3) (1996) 301–317.
20. Pitsch, H. and Steiner, H., Scalar mixing and dissipation rate in large-eddy simulations of nonpremixed combustion. *Proc. Combust. Inst.* **28** (2000) 35–40.
21. Stanley, S., Sarkar, S. and Mellado, J., A study of the flow field evolution and mixing in a planar turbulent jet using direct numerical simulations. *J. Fluid Mech.* **450** (2002) 377–407.
22. Schumann, U. and Sweet, R., A direct method for the solution of Poisson's equation with Neumann boundary conditions on a staggered grid of arbitrary size. *J. Comp. Phys.* **20** (1976) 171–182.
23. Smagorinsky, J., General circulation experiments with the primitive equations. 1. The basic experiment. *Monthly Weather Rev. 1* **91** (1963) 99–164.
24. Smirnov, A., Shi, S. and Celik, I., Random flow generation technique for large eddy simulations and particle-dynamics modeling. *J. Fluids Eng.* **123** (2001) 359–371.
25. Spalart, P., Direct numerical simulation of a turbulent boundary layer up to $Re_\phi = 1410$. *J. Fluid Mech.* **187** (1988) 61–98.
26. Tacke, M., Linow, S., Geis, S., Hassel, E., Janicka, J. and Chen, J.-Y., Experimental and numerical study of a highly diluted turbulent diffusion flame close to blowout. *Proc. Combust. Inst.* **27** (1998) 1139–1148.
27. Williamson, J., Low-storage Runge-Kutta schemes. *J. Comp. Phys.* **35** (1980) 48–56.